

Tuning the valley depolarization dynamics in selenium and vanadium alloyed monolayer MoS₂

Dipak Maity,^{1,*} Bhuvan Upadhyay^{①,2,3,*} Janmey Jay Panda^① Krishna Rani Sahoo^{①,†} Sreekant A.^① G. Rajalakshmi,¹ Suman Kalyan Pal,^{2,3,‡} and Tharangattu N. Narayanan^{①,§}

¹Materials and Interface Engineering Laboratory, Tata Institute of Fundamental Research Hyderabad, Serilingampally Mandal, Hyderabad 500046, India

²Advanced Materials Research Center, Indian Institute of Technology Mandi, Kamand, Mandi, Himachal Pradesh 175075, India

³School of Physical Sciences, Indian Institute of Technology Mandi, Kamand, Mandi, Himachal Pradesh 175075, India



(Received 19 February 2024; revised 16 May 2024; accepted 31 May 2024; published 24 June 2024)

The low valley polarization of monolayer transition-metal dichalcogenides at room temperature poses a significant obstacle to the development of valleytronic devices, and a mechanistic insight into the valley depolarization in such systems is still lacking. In this study, we demonstrate that substitutional doping leading to alloyed monolayers offer an effective strategy for enhancing valley polarization at room temperature. The degree of valley polarization, as determined by helicity-resolved transient absorption spectroscopy, is 15% for Se-doped and 30% for Se- and V-doped monolayer layer MoS₂ (referred to as MoSSe and VMoSSe, respectively). The valley polarization persists for longer durations in MoSSe (~15 ps) and VMoSSe (>500 ps) compared to pristine MoS₂ (~1 ps). The prolonged valley depolarization in MoSSe is attributed to a reduction in long-range electron-hole exchange interactions due to thermal mixing of bright and dark excitons. However, the valley depolarization in VMoSSe takes place via intervalley scattering of carriers between hybridized and defect excitons. Our study elucidates that altering the exciton ground state through the inclusion of additional levels near the conduction-band or valence band edges via alloying can enhance and prolong valley polarization in MoS₂. These findings are pivotal in realizing valleytronics devices at room temperature.

DOI: [10.1103/PhysRevMaterials.8.064004](https://doi.org/10.1103/PhysRevMaterials.8.064004)

I. INTRODUCTION

Valley engineering of semiconducting materials towards valleytronics applications is an emerging trend in materials science [1,2]. Semiconducting transition-metal dichalcogenides (TMDs) such as MoS₂, WS₂, WSe₂, etc. in monolayer limit are the potential systems in this venture due to their inherent inversion symmetry breaking ($E_{K\uparrow} \neq E_{K'\uparrow}$) and high spin-valley coupling [3–5]. This allows chirality-dependent valley-selective optical excitations and hence valley-selective polarizations with minimum intervalley cross talking [6,7]. Valley-based information processing needs valley splitting of the order of 25 meV for data retention and storage operations at room temperature [1]. This demands breaking of valley degeneracy; different approaches have been put forward for creating this [1,8]. Application of an external magnetic field, magnetic proximity effects, introduction of magnetic dopants to bring long-range ordering, etc. are some of the possible avenues explored in this juncture [9–11]. It has been shown by the authors that vanadium (V) doping is an efficient method for introducing the valley splitting in MoS₂ monolayers [12].

The effect of different concentrations of V doping can drastically change the electronic properties of MoS₂ monolayers [13]. Medium amount of V doping (~4 at. %) can keep the semiconducting (with an optical band gap of ~1.78 eV) properties of MoS₂ while bringing the band-gap differences at the *K* and *K'* valley points due to V-induced time-reversal symmetry breaking [12,13]. This has been proven by the differences in photoluminescence peaks (optical band gap calculated using *A*-exciton emission) as witnessed in our chirality-selective optical excitations [12]. Recent studies indicate that the most efficient method to break time-reversal symmetry is doping of various magnetic dopants such as Fe, Co, Ni, Cr, V, etc. [14–16]. Among them, only V doping can introduce efficient valley splitting in zero external magnetic field, enabling them for room-temperature valleytronics applications [12].

The enhancement of valley polarization is another important aspect of valleytronics where it is directly associated with the population differences among valleys [6,17]. Nayak *et al.* have reported 35 and 80% valley polarization for chemical vapor deposition (CVD)-grown WS₂ monolayers and bilayers, respectively at room temperature [18]. In a different work, Cao *et al.* have reported valley polarization up to 50% for MoS₂ [7]. We previously reported the polarization differences (*P*) of ~1% for MoS₂, ~1% for Se (~24 at. %)-doped MoS₂, ~42% for V-doped (~5 at. %) MoS₂, and ~10% for V (~2 at. %) and Se (~24 at. %)-codoped MoS₂ using chirality-selective photoluminescence (PL) studies with 532-nm excitation [12,19]. Liu *et al.* have recently reported a very high polarization ~50% for monolayer MoSSe alloy system

*These authors contributed equally to this work.

†Present address: Institute of Physics and Center for Nanotechnology, University of Münster, Wilhelm-Klemm-Str. 10, 48149 Münster, Germany.

‡Contact author: suman@iitmandi.ac.in

§Contact author: tnn@tifrh.res.in

[20]. Carrier concentration modulation by optical or electrical doping is also attempted to tune the valley polarization of TMD systems [21,22]. For example, Feng *et al.* have shown that valley polarization in WS_2 can be tuned by electrostatic and optical doping by applied bias and off-resonant laser excitation condition modulations [21]. In a different work, Shinokita *et al.* have shown that enhancing the valley polarization from 20 to 40% can be achieved by modulating the carrier density via biasing at lower temperatures (70 K) [22]. Similarly, with carrier tunability by applying bias, Back *et al.* have shown giant paramagnetic-field induced valley polarization in MoSe_2 [23]. Nonlinear valley Zeeman effect followed by enhancement in g factor leading to enhanced valley magnetic response was reported in WSe_2 [24]. All these systems achieved tunable valley polarization mostly by controlling the carrier concentration by external means and the studies are limited to PL-based ones. The presence of different types of defects, particularly in CVD-grown monolayer TMDs, makes it harder to predict the resonant conditions in PL studies as discussed in the following paragraphs.

The PL-based studies, as mentioned by the previous reports, have limitations in measuring the exact degree of valley polarization due to the possibilities of continuum-state excitations and interband scattering of electrons. Recent studies indicate that valley polarization at room temperature can be enhanced by modifying internal Coulomb forces and spin-orbit interactions in atomically thin TMDs via chalcogenide alloying, whereas they have shown high degree of valley polarization in $\text{Mo}(\text{S}_{0.8}\text{Se}_{0.2})_2$ unlike in MoS_2 and MoSe_2 at room temperature [20]. It has been stated that the mixing of dark and bright excitons is leading to the observed phenomenon in chalcogenide alloys [20]. But the roles of defects, valley selective relaxations, etc. need to be probed, opening up the possibilities for further investigations in this direction. Moreover, the extent of valley polarization in PL-based studied also depends on the energy of the pump used for excitation.

As mentioned above, previously many strategies like magnetic doping, magnetic field, magnetic proximity effects and optical pumping, defect engineering, and alloying were used for enhancing the valley polarization of TMDs [11,25]. Among them, most of the studies, including our previous studies, were based on PL measurements, where their limitations are discussed in our paper. Literature review indicates that a mechanistic insight in a valley polarization and depolarization dynamics in TMDs and their engineered systems are still lacking. Until now no extended studies have been made on the valley dynamics, especially when the ground state of conduction band (CB) or valence band (VB) is changed. The current paper addresses this lacuna using helicity-resolved transient absorption studies using the model systems such as monolayers of MoS_2 , Se-doped MoS_2 (MoSSe), and V along with Se-doped (alloyed) MoS_2 (VMoSSe). The valley dynamics of monolayer MoS_2 , MoSSe (Se-doped MoS_2 where the at. % of Se amount is found as $\sim 19\%$, using x-ray photoemission spectroscopy analyses), and VMoSSe (V and Se co-doped MoS_2 , where the V and Se amounts are found as ~ 3 and $\sim 20\%$, respectively) systems are studied using polarization-dependent transient absorption (TA) studies. Utilizing helicity-resolved TA spectroscopy, we observed an

increase in valley polarization for alloys that lasted longer than single-layer MoS_2 . Furthermore, we comprehended the valley dynamics and provided a plausible explanation for the enhanced valley lifetime, attributing it to the alterations in the band structure introduced by the doping process.

II. EXPERIMENTAL METHODS

A. MoS_2 , MoSSe , and VMoSSe synthesis

Monolayer MoS_2 , MoSSe , and VMoSSe are synthesized over Si/SiO_2 substrate using CVD-assisted method, as discussed in our previous papers [13,19,26]. The schematic of the synthesis process is illustrated in Fig. S1 of the Supplemental Material [27] information. In this method, MoO_3 and V_2O_5 powders are used as precursors. Sulfur and selenium powders are used as sulfur and selenium sources. To enable the growth process, a carrier gas mixture of Ar/H_2 is used. For the MoS_2 growth the temperature on the sulfur side is maintained at 210°C , while the temperature on the precursor side is set to 710°C . For the case of MoSSe and VMoSSe , the temperatures on the selenium side and precursor side are kept at 400 and 780°C , respectively. The temperature ramp time and growth time for all the growth are 30 min and 15 min. The gas-flow rate during the MoS_2 synthesis is 190 sccm and that for the MoSSe and VMoSSe synthesis is 200 sccm.

B. Experimental techniques

Optical images of thin samples are captured using an optical microscope, while a Renishaw Invia micro-Raman spectrometer with 532-nm excitation wavelength, L50 \times objective lens, and 2400-gr/mm grating with 0.50 N.A. is used to capture Raman and PL spectra. The chirality-resolved emission following a linear polarized excitation (wavelength 532 nm) is detected from the samples using a quarter-wave plate and a polarizer. The morphology of the samples is measured using scanning electron microscopy (SEM, JEOL FESEM JSM 7200). A homemade setup is used for transient absorption measurements. A light beam (800 nm) obtained from a laser amplifier (Spit fire Ace, Spectra Physics), with output power 4 W, pulse width <35 fs, and a repetition rate 1 kHz, is used as a source. A focused beam (800 nm) through a sapphire crystal is used to generate white-light continuum probe. Two parametric amplifiers (TOPAS Prime from Light Conversion) are used for generating different pump and probe wavelengths. TA spectra are collected by charge-coupled device arrays fitted with a grating spectrograph (Acton spectra Pro SP 2358). TA kinetic traces are obtained through two well-aligned photodiodes of variable gain. We use Fresnel rhomb retarders, FR600QM and FR600HM, manufactured by Thorlabs, as quarter- and half wave plates, respectively. The laser output from TOPAS is linearly polarized. We keep the optical axis of the retarder, FR600QM (quarter wave plate) at 45° for obtaining circular polarized light. During experiment, we fix the helicity of the pump beam for specifically exciting the K valley. But, probe helicity is changed for obtaining the carrier dynamics of K and $-K(K')$ valleys. We used a retarder, FR600HM (half wave plate) before the quarter wave plate for changing the helicity of the probe.

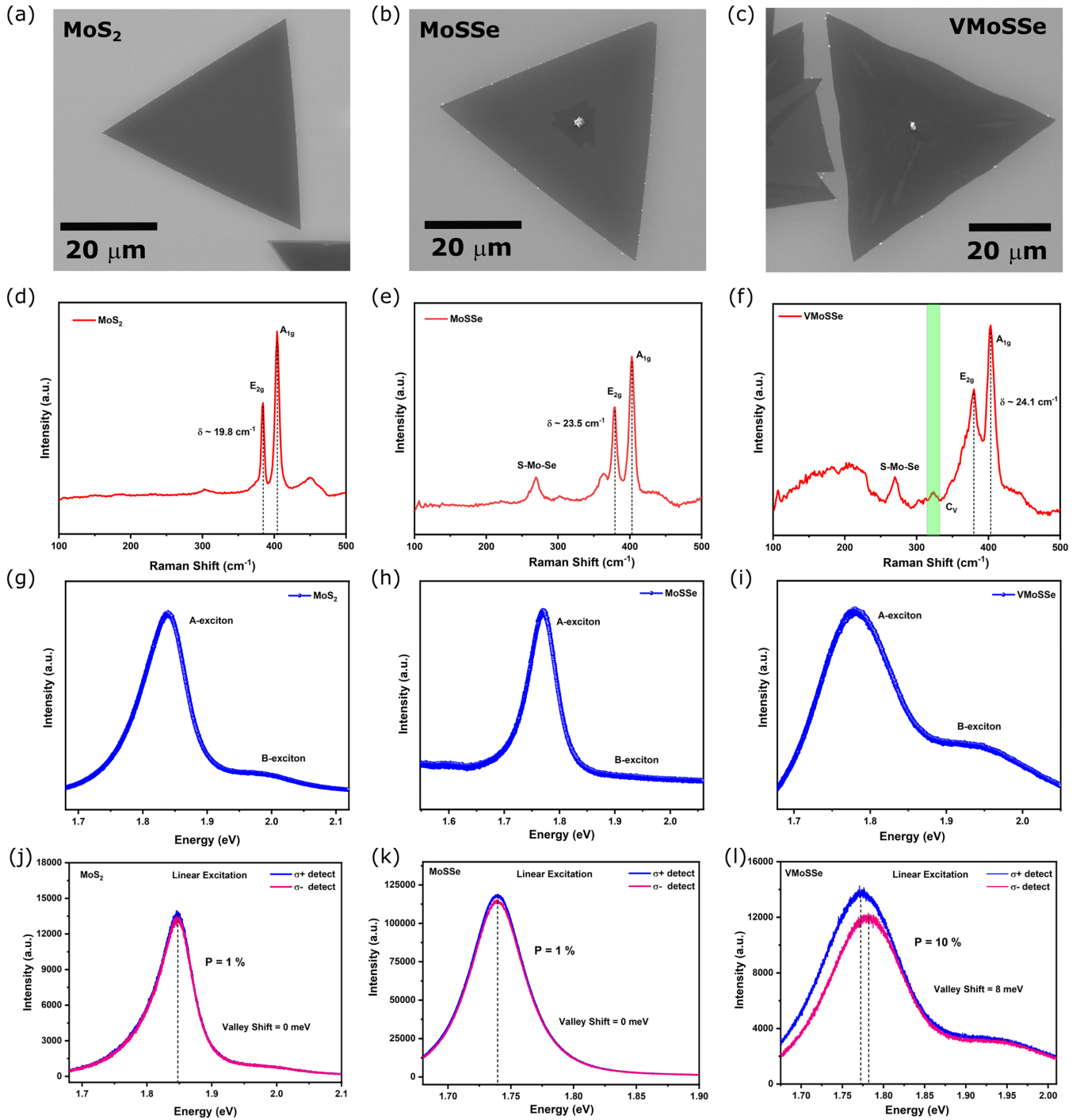


FIG. 1. SEM images of monolayers of: (a) MoS₂ (b) MoSSe, and (c) VMoSSe alloy crystals, indicating the formation of triangular monolayer crystals. The central part of the MoSSe has multiple layers but this region is not considered for experiments. The white particles are MoO₃. Raman spectra of (d) MoS₂ (e) MoSSe, and (f) VMoSSe crystals indicating the characteristics phonon modes, as discussed in the text. PL spectra of (g) MoS₂, (h) MoSSe, and (i) VMoSSe at an excitation wavelength of 532 nm. The excitation is carried out with linear polarization, and PL detection is not chirality resolved. The A excitons are prominent in all the crystals but as the defect increases, its intensity decreases leading to the appearance of B exciton. Chirality-selective PL spectra using linearly polarized optical excitation using 532-nm light and detection of σ^+ and σ^- in the output of (j) MoS₂, (k) MoSSe, and (l) VMoSSe [19]. The experimental details have been discussed in our previous work [19].

III. RESULTS AND DISCUSSION

Monolayers of MoS₂, MoSSe, and VMoSSe are synthesized using CVD technique, as discussed in our previous

papers [13,19]. Figures 1(a)–1(c) show the SEM images of MoS₂, MoSSe, and VMoSSe, indicating the formation of crystals of sizes (lateral widths) ~ 50 , ~ 60 , and ~ 50 μm , respectively, over Si/SiO₂ substrate. Figures 1(d)–1(f) indicate

the Raman spectra of these samples, and the features of the individual spectra are presented briefly here.

Raman spectrum of MoS₂ shows two characteristic modes, E_{2g} (in-plane vibration) and A_{1g} (out-of-plane vibration) at ~ 384 and ~ 404 cm⁻¹, respectively. The difference between E_{2g} and A_{1g} modes is found to be ~ 20 cm⁻¹, indicating the formation of a single layer [28]. In MoSSe, in addition to the characteristic Raman modes of MoS₂, another Raman active mode at ~ 267 cm⁻¹ is observed. This mode arises from the vibrations of partially selenized MoS₂. Despite being a monolayer, the MoSSe layer exhibits a separation of approximately 23 cm⁻¹ between the E_{2g} and A_{1g} modes.

The increased separation is due to strain effects induced in the lattice by Se doping, as demonstrated in previous reports [13,29]. Furthermore, in VMoSSe, an additional small peak at 325 cm⁻¹ is observed in the Raman spectrum. This peak is a characteristic mode that emerges due to vanadium (C_v peak) atoms doped into the MoSSe lattice and its intensity is sensitive to the doping concentration [12,30]. Apart from this, as the vanadium atoms are introduced as dopants, a set of peaks begins to emerge in the range of 100–230 cm⁻¹, which was previously reported to be associated with defect-site related phonon modes [13,31]. In VMoSSe, the position of the E_{2g} peak is slightly redshifted, while the position of the A_{1g} peak remains unaffected. The separation between E_{2g} and A_{1g} modes is approximately ~ 24 cm⁻¹, which can be attributed to the additional strain induced by vanadium doping [12,13]. Figures 1(g)–1(i) show the PL spectra of MoS₂, MoSSe, and VMoSSe with 532-nm excitation indicating two emission peaks corresponding to A exciton (dominating one) and B exciton (small peak).

The chirality-selective PL studies conducted with 532-nm excitation [Figs. 1(j)–1(l)], as reported in our previous works, indicate large differences in the emission (intensity and broadness) with the variations in the range of dopants (with the variations in V amount), nature of dopants (Se or V), and with the changes in defects (postsulfurization (plasma) treatment vs as-prepared MoS₂) [12,19]. Previous studies also demonstrated substrate-dependent differences in chirality-selective PL. The room-temperature PL spectrum of MoS₂ shows the asymmetry nature [Fig. 1(j)], suggesting formation of trion. To get the accurate value of intensity difference (P), we fit both the spectra of MoS₂ and find the value of $P \sim 2\%$ (Fig. S3 [27]), although both the peak positions remain the same, whereas the V and Se doping in MoS₂ affects the PL differently where both peak positions and intensities behave differently [Figs. 1(j)–1(l)]. Room-temperature PL position shifts of ~ 35 and 8 meV are occurring for V-MoS₂ (~ 5 at. % V) and V-MoSSe (~ 2 at. % V) while there no such shifts occurring in MoS₂ and MoSSe [12,19]. Differences in the area and intensity of PL spectra at two different chiral excitations are occurring with extension of Se doping or post-treatment of MoS₂ with plasma or further sulfur annealing [12,19]. Though these studies indicate that the PL position shifts are due to the valley position shifts occurring due to time-reversal symmetry breaking by the doping of V, such studies are inadequate to comment on exact behavior of valley polarizations. Intervalley scattering, defect-mediated spin relaxation, defect-induced variations in carrier dynamics, etc. cannot be understood with the existing studies [32,33].

The dynamics of charge carriers that governs the optoelectronic properties of semiconductors, particularly monolayers of TMDs such as MoS₂, can be largely affected by the defects. For example, though emissions from both A - and B excitons (those emissions due to the recombination of electrons in the conduction band with holes in the spin-orbit split-valence bands) [34] are highly likely in MoS₂; the intensity variations among them can occur due to increase of nonradiative recombination with the extension of defects. Hence the intensity ratio of B and A (I_B/I_A) can be used as a measure of the quality of the crystal, with low ratio indicating low defect density. Studies indicate that an expected lifetime of ~ 800 ps can be assigned to the A exciton in MoS₂ at room temperature but that of B exciton is quite short (~ 10 ps), where the radiative recombination is highly affected by temperature [34]. Due to additional relaxation pathways of B exciton to A exciton, in defect-free(less) systems, a high intensity of A -exciton emission is expected, as we have seen in the PL of pristine MoS₂ [Fig. 1(g)]. The nonradiative pathways, impacted by charge trapping in defects, exciton-exciton annihilation, etc., occur in much shorter timescale (~ 10 ps for A) and hence A -exciton intensity is more largely affected by defects than those of B exciton [34]. Hence, to calculate the valley polarization in doped TMDs, carrier dynamics need to be studied and pump-probe spectroscopy is ideal for such studies. Since the optical selection rules allow selective valley excitation with circular polarized lights in monolayer MoS₂, chirality-selective valley excitations and probing using same or different chirality probe beams are carried out here.

Figure 2(a) illustrates the transient absorption (TA) spectra for monolayer MoS₂ having bleach bands at 675 and 610 nm corresponding to A - and B -excitonic transitions, respectively. However, the TA spectra of MoS₂ are modified following selenium- (Se) and vanadium (V) doping. In the TA spectra of MoSSe [Fig. 2(b)], two bleach bands are observed at 640 nm (G band) and 710 nm (H band). Conversely, in the case of VMoSSe [Fig. 2(c)], there are three bleach bands: X (at 730 nm), Y (at 670 nm), and Z (at 575 nm) in the TA spectra. The bleach bands in VMoSSe are broader than those of MoS₂ and MoSSe. We compare linear absorption spectra of these samples to understand the difference in TA spectra (Fig. S4(a) [27]). While A - and B bands are narrow in MoS₂ and MoSSe, these bands become wider in VMoSSe. This linewidth broadening is attributed to the induction of induced defects states and strong carrier-phonon coupling in VMoSSe [35]. Therefore, the broad and redshifted bleach bands in the TA spectra of V-doped sample could arise from defect-induced linewidth broadening and transitions from conduction band to dopant-related defect states [33].

To investigate the difference between valley properties of doped TMDs and MoS₂, helicity-resolved (HR) TA kinetics measurements are conducted. It is essential to note that the time resolution of the HRTA measurements is worse (0.3 ps) than that of the TA measurements (60 fs) due to the utilization of prism quarter wave plates (Fig. S4(b) [27]). Figure 3(a) shows the HRTA kinetics for the A exciton in MoS₂, measured with a pump light of 660 nm, in close proximity to the A -exciton level. The degree of valley polarization (DOP) can be calculated from TA kinetics measured with same circular

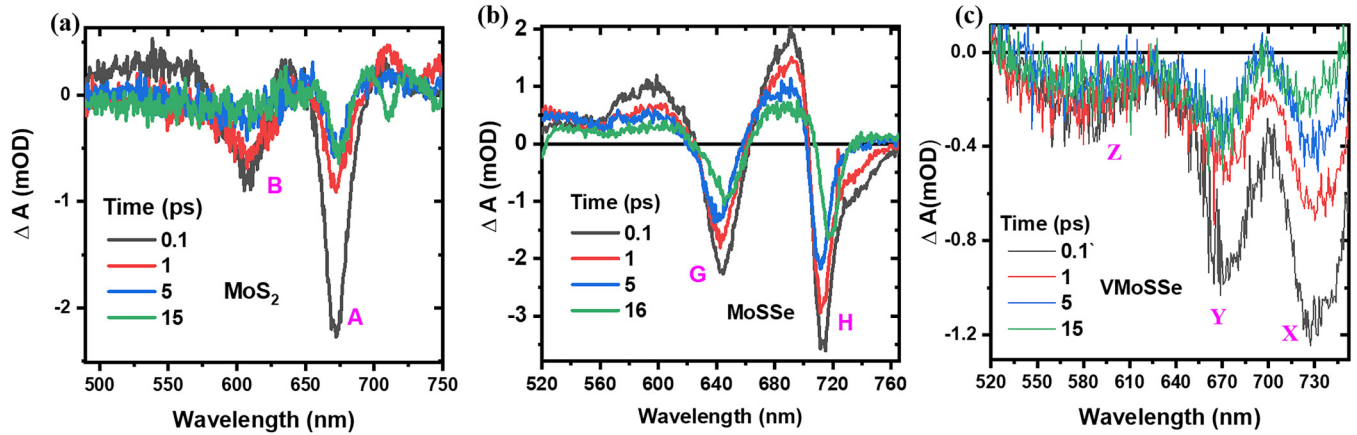


FIG. 2. Evolution of TA spectra with time for (a) MoS₂, (b) MoSSe, and (c) VMoSSe. The TA spectra were measured with 480-nm pump light.

polarisation (SCP) and opposite circular polarisation (OCP) pump and probe beams using the following equation:

$$\text{DOP (\%)} = \frac{\Delta A_{\text{SCP}} - \Delta A_{\text{OCP}}}{\Delta A_{\text{SCP}} + \Delta A_{\text{OCP}}} \times 100, \quad (1)$$

where ΔA_{SCP} and ΔA_{OCP} are the transient absorption signals for same and opposite circular polarisation of pump and probe beams, respectively. The maximum value of the degree of valley polarisation of MoS₂ is found to be around 5% (Fig. S5(a) [27]), which undergoes a fast (~ 1 ps) depolarization. Subsequently, the HRTA kinetics were measured with a pump wavelength of 710 nm and probed near the H-band (720 nm) for the MoSSe alloy (Fig. 3(b)). In contrast to MoS₂, the TA kinetics for SCP significantly differ from OCP in MoSSe, resulting in a high DOP (15%), which persists for approximately ~ 15 ps (Fig. S5(a) [27]). Similarly, SCP and OCP kinetics were recorded for VMoSSe by probing close to the defect band (at 715 nm) following an excitation at 690 nm (Fig. 3(c)). Interestingly, the highest DOP (30%) is achieved in VMoSSe, and the valley polarization endures for a more extended period (not decaying to zero until 500 ps) compared to the other two TMDs (Fig. S5(b) [27]).

The dynamics of valley depolarization can be analyzed from the time evolution of the difference between the SCP and OCP TA signals [36,37]. In Fig. 4(a), we present the calculated difference signal (ΔA_d) from the SCP and OCP TA signals for monolayer MoS₂, MoSSe, and VMoSSe. For MoS₂, the difference in signal was fitted with a single exponential function, yielding a lifetime of 0.45 ± 0.13 ps. Previously, valley polarization of monolayer MoS₂ was investigated, revealing two processes involved in valley dynamics at room temperature: one was faster exciton spin precession (< 100 fs) and the other was excess carrier decay in the valley (≤ 1 ps) [36]. Although the time resolution of our measurements did not allow us to observe the fast decay time (~ 100 fs), the observed lifetime of 0.45 ps (τ_{VS}) could be associated with excess carrier decay via intervalley scattering. This intervalley scattering process is depicted schematically in Fig. 4(b). Here, τ_{VS} denotes the intervalley scattering lifetime for bright excitons. The atomically thin nature of TMDs leads to a robust electrostatic interaction between electrons and holes [20]. As a result, a substantial overlap of wave functions occurs between electrons and holes [20]. The consequence is a high electron-hole exchange interaction between the valleys, leading to intervalley scattering [20].

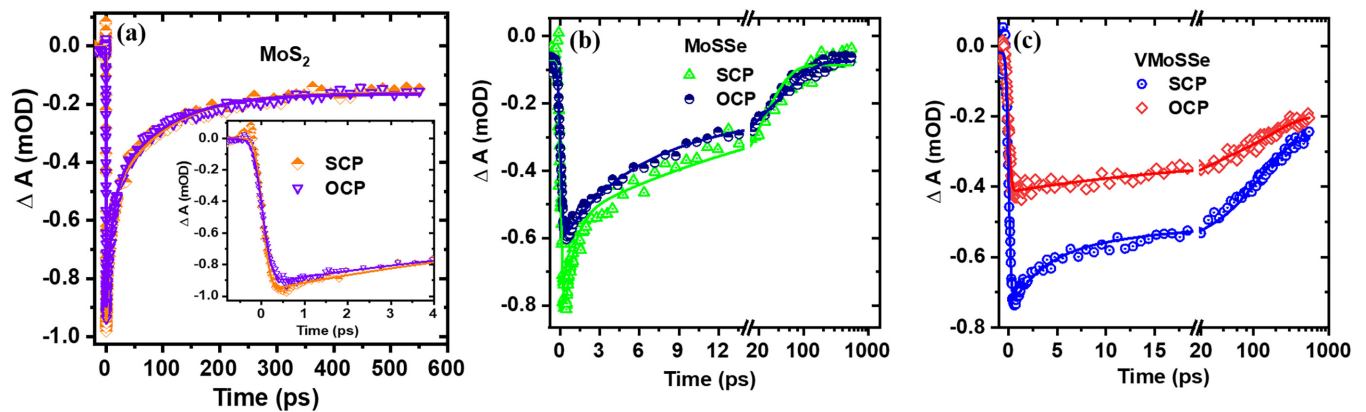


FIG. 3. (a) Helicity-resolved transient absorption TA kinetics of MoS₂ measured with pump beam of 660 nm. Inset: Evolution of helicity-resolved TA kinetics at short delay times. SCP (OCP) represents the same (opposite) circular polarization of pump and probe beams. Helicity-resolved TA kinetics for (b) MoSSe (pump wavelength ~ 710 nm) and (c) VMoSSe (pump wavelength ~ 715 nm). Log scale is used after 20 ps.

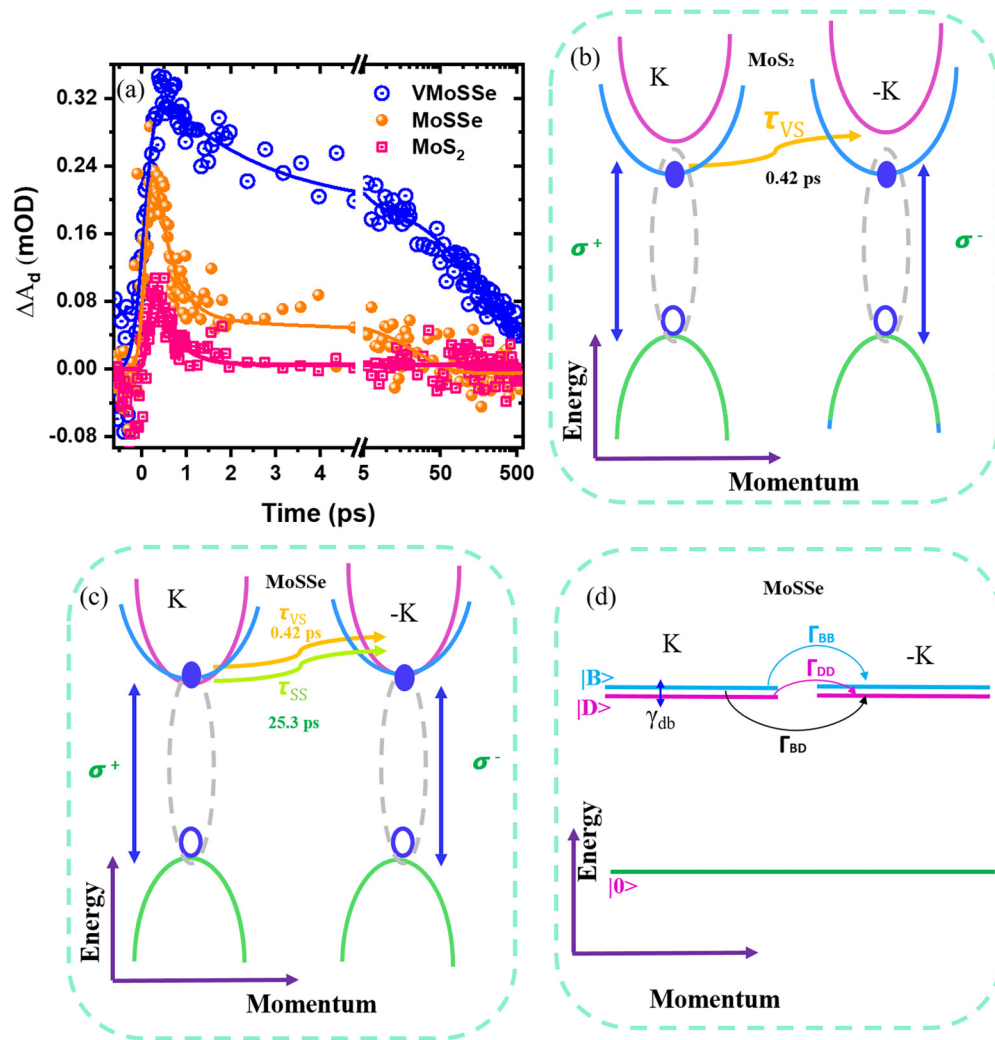


FIG. 4. (a) The evolution of the difference (ΔA_d) between the SCP and OCP signals with pump-probe delay. Schematics illustrating the valley depolarization processes after optical excitation in the K valley in monolayer layer (b) MoS₂, and (c) MoSSe. The pink and blue color parabolas represent CB levels corresponding to the dark and bright excitons, respectively. τ_{SS} is the scattering time of the carriers due to mixing of bright and dark states. (d) The sketch depicts the possible intravalley and intervalley scattering of exciton in MoSSe. $|0\rangle$, $|B\rangle$, and $|D\rangle$ denote ground state, bright-, and dark exciton state, respectively. Here, γ_{db} is intravalley scattering rate. Γ_{BB} , Γ_{DD} , and Γ_{BD} represent the times of intervalley bright-bright, dark-dark, and bright-dark exciton scattering, respectively.

The biexponential fitting of the decay of difference signal (ΔA_d) for MoSSe [Fig. 4(a)] yields two lifetime components: 0.42 ± 0.06 ps (81%) and 25.26 ± 8.73 ps (19%). Similar to MoS₂, the faster decay component likely represents carrier decay via intervalley scattering between the bright exciton. It has been reported that Se doping in MoS₂ alters spin-orbit interactions, and the energetic ordering of the fine structure of excitonic levels (bright and dark) changes [20]. Moreover, an earlier report suggests that around 20% Se doping in MoS₂ can result in mixed excitonic states, where the energy splitting (Δ_{db}) between dark and bright exciton states is nearly zero [20]. Wang *et al.* reported that the intravalley relaxation time of the exciton is of the same order as intervalley scattering, and these relaxations are much faster when the splitting between levels is low, leading to instantaneous bright-to-dark exciton relaxation [38]. In the case of the spin-forbidden dark exciton, the absence of long-range electron-hole exchange interactions inhibits the fast depolarization of valley [20].

The thermal mixing of bright and dark excitons can lead to a reduction in electron-hole exchange interactions [20]. Therefore, the longer lifetime (~ 25 ps) for MoSSe could be attributed to the decay of carriers in mixed states (dark and bright exciton) via intervalley scattering. The processes of bright-exciton intervalley scattering (lifetime τ_{VS}) and carrier scattering in mixed states (lifetime τ_{SS}) are illustrated in Fig. 4(c). To elaborate, valley depolarization dynamics in MoSSe is governed by both intravalley- and intervalley scattering of excitons [Fig. 4(d)]. In a previous study, the intravalley scattering rate from the dark to bright state was reported as $\gamma_{db} = 1\text{ps}^{-1}$ [35]. However, the scattering from dark to bright excitons via thermal excitation can be described by $\gamma_{db} \exp(-\frac{|\Delta E|}{kT})$, where it depends upon the energy splitting (ΔE) between the bright and dark excitons and temperature [35]. Consequently, this scattering rate may increase even further at room temperature as the energy splitting diminishes. In typical TMDs, the exciton ground state is usually either

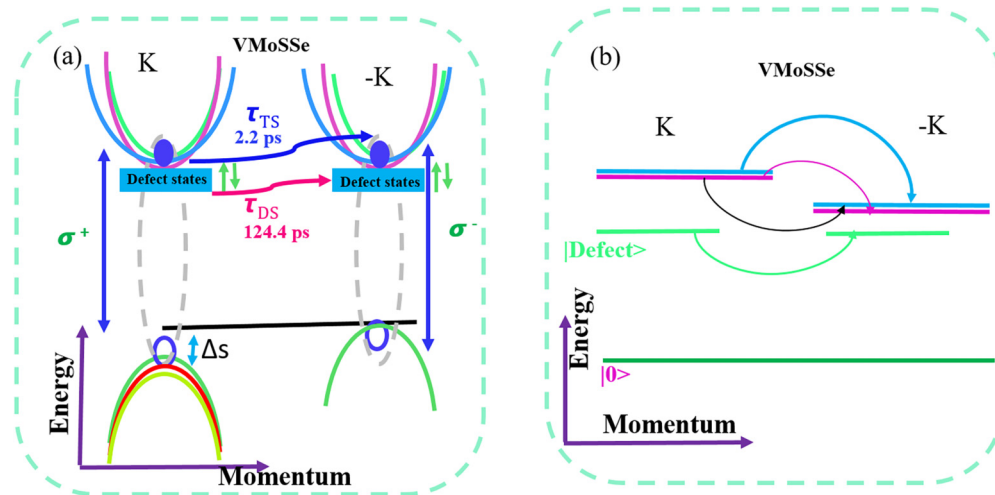


FIG. 5. (a) Schematics illustrating the valley depolarization processes after optical excitation in the K valley in monolayer layer VmoSSe, where ΔS represents the energy shift (8 meV) of $-K$ valley with respect to K as a result of time-reversal symmetry breaking. The pink and blue color parabolas represent the dark and bright exciton levels, respectively. τ_{TS} is the intervalley scattering time of the hybrid excitons and τ_{DS} denotes scattering time of the defect bound excitons. (b) The sketch depicts the possible intervalley scattering of excitons having mixed bright–dark–defect character in VMoSSe.

a bright or a dark state. However, MoSSe exhibits a unique exciton ground state, resulting from the mixing of CB levels, which combines characteristics of both bright and dark states. As a result, intervalley scattering in MoSSe can occur through three distinct mechanisms: (1) bright-bright (B-B), (2) dark-dark (D-D), and (3) bright-dark (B-D) exciton scatterings. It has been noted that B-B exciton intervalley scattering occurs very rapidly, with a scattering time of 0.4 ps. Conversely, the scattering processes involving D-D and B-D excitons are comparatively slower. Specifically, the D-D exciton scattering time was reported to be approximately 70 ps [35]. The observed 25-ps lifetime likely represents the scattering time of B-D excitons. Therefore, the sluggish nature of B-D and D-D exciton scattering can result in high valley polarization of MoSSe at room temperature.

Next, we fitted the dynamics of ΔA_d for VMoSSe [Fig. 4(a)] and obtained two lifetimes: 2.22 ± 0.44 ps (51%) and 124.42 ± 20.89 ps (49%). As the kinetics of ΔA_d is very different compared to MoSSe, the carrier dynamics in VMoSSe is expected to be dominated by the vanadium-induced states. Recently, theoretical calculations on monolayer TMDs with point defects reported strong hybridization between the A exciton and defect excitons, leading to changes in valley and optical properties [39]. According to these calculations, excitonic optical transitions between the defect states and the pristine crystal state possess the circular dichroism selectivity [39]. However, both A and B excitons in the pristine monolayer can significantly mix with transitions involving the defect states, causing broadening of absorption spectrum [39]. We observed broadening in the linear absorption (Fig. S4(a) [27]) and bleach band of TA [Fig. 2(c)] spectra of VMoSSe, which could be attributed to the mixing of untrapped and trapped transitions. This is further supported by our density-functional theory calculations that suggested the introduction of vanadium states near the CB and VB edges [19]. As we measured TA kinetics at 715 nm, the calculated valley polarization is not for the

pure A exciton but for hybridized or defect excitons. The longer lifetime (~ 124 ps) could be associated with the decay of excess defect excitons from defect levels introduced by V doping [40,41], supported by a previous study on monolayer WSe₂ with chalcogen vacancies, by Moody *et al.* [40]. They found long-lived valley polarization and microsecond valley scattering time from time-resolved PL measurements that was interpreted as originated from defect excitons [40]. Figure 5(a) illustrates the valley depolarization processes after optical excitation in the K valley in monolayer VMoSSe. Nonetheless, the shorter decay time (2.22 ps) of the difference signal could possibly be assigned to the intervalley scattering of hybridized excitons. In VMoSSe, the faster valley depolarization time is 5 times longer than that of MoS₂ or MoSSe (~ 0.4 ps). Such differences can arise due to multiple reasons, such as (1) time-reversal symmetry breaking (TRSB) of valleys in VMoSSe, as evidenced from Fig. 1(i); (2) the intravalley transition between the different energy states of VB and CB; (3) hybridized excitons near defect levels inhibiting the free movement of excitons via localization, preventing long-range electron-hole exchange interactions [39]; and (4) possible alteration of the spin-orbit interactions of exciton levels, which also impact valley polarization. The possible intervalley scattering of the carriers in the hybrid (scattering time, τ_{TS}) and the defect (scattering time, τ_{DS}) excitons are shown in Fig. 5(a). Furthermore, Fig. 5(b) depicts all the possible scattering routes responsible for valley depolarization in VMoSSe. TRSB induces an approximately 8 meV shift in the VB edge of the $-K$ valley of VMoSSe. Simultaneously, the introduction of states (due to V doping) near the VB and CB edges at the K valley triggers a modification in the exciton ground states [19]. These altered exciton states, possessing comparable energy levels at both the K and $-K$ valleys, can undergo intervalley scattering. Furthermore, the change in energy-level alignment in both valleys can lead to the transition of the exciton ground state from bright to dark, resulting in distinctive intervalley scattering behaviors.

Consequently, TRSB and the emergence of energy states near the VB and CB levels collectively give rise to multiple intervalley scattering pathways between the K and $-K$ valleys. Some of these scattering routes exhibit slower dynamics compared to bright-exciton intervalley scattering, thereby leading to an extended valley depolarization lifetime [42]. In a nutshell, changes in the character of exciton ground state along with localization of exciton by defect states leads to high and long-lived valley polarization in VMoSSe.

The steady-state valley DOP (P_c) is related to the valley scattering time according to the equation [40]

$$P_c = \frac{P_0}{\left(1 + \frac{\tau}{\tau_s}\right)}, \quad (2)$$

where P_0 , τ , and τ_s represent the valley DOP immediately after photoexcitation, the recombination time of carriers and the intervalley scattering time, respectively. By utilizing $P_0 = 30\%$ (DOP at 0.3 ps) and $P_c = 10\%$ (DOP at 550 ps in Fig. S5(b) [27]), we determine that $\tau_s = \tau/2$ for VMoSSe. This implies that the valley scattering time is equal to half the decay time of trapped carriers. These observations infer that trapped excitons in the defect states exhibit a long valley scattering time, leading to long-lived valley polarization in VMoSSe.

IV. CONCLUSIONS

In summary, we employed helicity-resolved TA spectroscopy to investigate the valley polarization in monolayer MoS₂, MoSSe, and VMoSSe. A notably high valley polarization is achieved at room temperature in monolayer MoS₂ through substitutional (Mo/S) doping using V/Se. The

maximum values of the DOP achieved for MoS₂, MoSSe, and VMoSSe are 5, 15, and 30%, respectively. While valley depolarization in MoS₂ and MoSSe is attributed to carrier decay via intervalley scattering between bright excitons, in VMoSSe it occurs through carrier scattering in mixed exciton states (bright/dark) induced by Se and V doping. Moreover, the valley polarization in VMoSSe is much longer lived (>500 ps) than the other two materials, owing to the involvement of V-doping related defect excitons. The prolonged intervalley scattering lifetime (~ 124 ps) for the hybridized (defect) excitons contributes to slower valley depolarization in VMoSSe, making V-doped MoSSe a promising candidate for valleytronics applications at room temperature. These findings offer insights into the design of TMD-based valleytronics materials through different doping strategies.

ACKNOWLEDGMENTS

D.M., J.J.P., K.R.S., S.A., G.R., and T.N.N. of Tata Institute of Fundamental Research Hyderabad (TIFR) acknowledge the support of the Department of Atomic Energy, Government of India, under Project Identification No. RTI4007. T.N.N. and G.R. acknowledge the support from SERB-SUPRA (Grant No. SPR/2020/000220) project entitled “*Development of Spin-correlation Engineered Transition Metal Dichalcogenides and Novel Light-assisted Methods for Probing them.*” The authors thank the Advanced Materials Research Centre (AMRC), IIT Mandi for providing experimental facilities. S.K.P. acknowledges the financial support via a research grant (Grant No. CRG/2018/003045) from the Science and Engineering Research Board (SERB), Government of India. B.U. thanks the Ministry of Education of India for providing a fellowship.

-
- [1] S. A. Vitale, D. Nezich, J. O. Varghese, P. Kim, N. Gedik, P. Jarillo-Herrero, D. Xiao, and M. Rothschild, Valleytronics: Opportunities, challenges, and paths forward, *Small* **14**, 1801483 (2018).
- [2] D. Xiao, G.-B. Liu, W. Feng, X. Xu, and W. Yao, Coupled spin and valley physics in monolayers of MoS₂ and other group-VI dichalcogenides, *Phys. Rev. Lett.* **108**, 196802 (2012).
- [3] E. S. Kadantsev and P. Hawrylak, Electronic structure of a single MoS₂ monolayer, *Solid State Commun.* **152**, 909 (2012).
- [4] Z. Y. Zhu, Y. C. Cheng, and U. Schwingenschlöggl, Giant spin-orbit-induced spin splitting in two-dimensional transition-metal dichalcogenide semiconductors, *Phys. Rev. B* **84**, 153402 (2011).
- [5] H. Zeng, G.-B. Liu, J. Dai, Y. Yan, B. Zhu, R. He, L. Xie, S. Xu, X. Chen, W. Yao, and X. Cui, Optical signature of symmetry variations and spin-valley coupling in atomically thin tungsten dichalcogenides, *Sci. Rep.* **3**, 1608 (2013).
- [6] K. F. Mak, K. He, J. Shan, and T. F. Heinz, Control of valley polarization in monolayer MoS₂ by optical helicity, *Nat. Nanotechnol.* **7**, 494 (2012).
- [7] T. Cao, G. Wang, W. Han, H. Ye, C. Zhu, J. Shi, Q. Niu, P. Tan, E. Wang, B. Liu, and J. Feng, Valley-selective circular dichroism of monolayer molybdenum disulfide, *Nat. Commun.* **3**, 887 (2012).
- [8] W. Yao, D. Xiao, and Q. Niu, Valley-dependent optoelectronics from inversion symmetry breaking, *Phys. Rev. B* **77**, 235406 (2008).
- [9] Y. Li, J. Ludwig, T. Low, A. Chernikov, X. Cui, G. Arefe, Y. D. Kim, A. M. Zande, A. Rigosi, H. M. Hill, S. H. Kim, J. Hone, Z. Li, D. Smirnov, and T. F. Heinz, Valley splitting and polarization by the Zeeman effect in monolayer MoSe₂, *Phys. Rev. Lett.* **113**, 266804 (2014).
- [10] D. Macneill, C. Heikes, K. F. Mak, Z. Anderson, A. Kormányos, V. Zólyomi, J. Park, and D. C. Ralph, Breaking of valley degeneracy by magnetic field in monolayer MoSe₂, *Phys. Rev. Lett.* **114**, 037401 (2015).
- [11] K. L. Seyler, D. Zhong, B. Huang, X. Linpeng, N. P. Wilson, T. Taniguchi, K. Watanabe, W. Yao, D. Xiao, M. A. McGuire, K.-M. C. Fu, and X. Xu, Valley manipulation by optically tuning the magnetic proximity effect in WSe₂/CrI₃ heterostructures, *Nano Lett.* **18**, 3823 (2018).
- [12] K. R. Sahoo, J. J. Panda, S. Bawari, R. Sharma, D. Maity, A. Lal, R. Arenal, G. Rajalaksmi, and T. N. Narayanan, Enhanced room-temperature spin-valley coupling in V-Doped MoS₂, *Phys. Rev. Mater.* **6**, 085202 (2022).
- [13] D. Maity, R. Sharma, K. R. Sahoo, A. Lal, R. Arenal, and T. N. Narayanan, On the existence of photoluminescence and room-temperature spin polarization in ambipolar V Doped MoS₂ monolayers, *arXiv:2204.05887*.

- [14] W. F. Li, C. Fang, and M. A. Van Huis, Strong spin-orbit splitting and magnetism of point defect states in monolayer WS₂, *Phys. Rev. B* **94**, 195425 (2016).
- [15] S. Fu, K. Kang, K. Shayan, A. Yoshimura, S. Dadras, X. Wang, L. Zhang, S. Chen, N. Liu, A. Jindal, X. Li, A. N. Pasupathy, A. N. Vamivakas, V. Meunier, S. Strauf, and E.-H. Yang, Enabling room temperature ferromagnetism in monolayer MoS₂ via in situ iron-doping, *Nat. Commun.* **11**, 6 (2020).
- [16] Q. Li, X. Zhao, L. Deng, Z. Shi, S. Liu, Q. Wei, L. Zhang, Y. Cheng, L. Zhang, H. Lu, W. Gao, W. Huang, C.-W. Qiu, G. Xiang, S. J. Pennycook, Q. Xiong, K. P. Loh, and B. Peng, Enhanced valley Zeeman splitting in Fe-doped monolayer MoS₂, *ACS Nano* **14**, 4636 (2020).
- [17] Z. Zhu, A. Collaudin, B. Fauqué, W. Kang, and K. Behnia, Field-induced polarization of Dirac valleys in bismuth, *Nat. Phys.* **8**, 89 (2012).
- [18] P. K. Nayak, F. C. Lin, C. H. Yeh, J. S. Huang, and P. W. Chiu, Robust room temperature valley polarization in monolayer and bilayer WS₂, *Nanoscale* **8**, 6035 (2016).
- [19] D. Maity, R. Sharma, K. R. Sahoo, J. J. Panda, A. Lal, A. B. Puthirath, P. M. Ajayan, and T. N. Narayanan, On the electronic and spin-valley coupling of vanadium doped MoS_{2(1-x)}Se_{2x} monolayers, *J. Phys.: Condens. Matter* **35**, 505002 (2023).
- [20] S. Liu, A. G. del Águila, X. Liu, Y. Zhu, Y. Han, A. Chaturvedi, P. Gong, H. Yu, H. Zhang, W. Yao, and Q. Xiong, Room-temperature valley polarization in atomically thin semiconductors via chalcogenide alloying, *ACS Nano* **14**, 9873 (2020).
- [21] S. Feng, C. Cong, S. Konabe, J. Zhang, J. Shang, Y. Chen, C. Zou, B. Cao, L. Wu, N. Peimyoo, B. Zhang, and T. Yu, Engineering valley polarization of monolayer WS₂: A physical doping approach, *Small* **15**, 1805503 (2019).
- [22] K. Shinokita, X. Wang, Y. Miyauchi, K. Watanabe, T. Taniguchi, and K. Matsuda, Continuous control and enhancement of excitonic valley polarization in monolayer WSe₂ by electrostatic doping, *Adv. Funct. Mater.* **29**, 1900260 (2019).
- [23] P. Back, M. Sidler, O. Cotlet, A. Srivastava, N. Takemura, M. Kroner, and A. Imamoğlu, Giant paramagnetism-induced valley polarization of electrons in charge-tunable monolayer MoSe₂, *Phys. Rev. Lett.* **118**, 237404 (2017).
- [24] Z. Wang, K. F. Mak, and J. Shan, Strongly interaction-enhanced valley magnetic response in monolayer WSe₂, *Phys. Rev. Lett.* **120**, 066402 (2018).
- [25] Y. Xu, Y. Wang, S. Wang, S. Yu, B. Huang, Y. Dai, and W. Wei, Spontaneous valley polarization caused by crystalline symmetry breaking in nonmagnetic LaOMX₂ monolayers, *Nano Lett.* **22**, 9147 (2022).
- [26] D. Maity, M. Sahoo, K. R. Sahoo, S. K. Nayak, T. N. Narayanan, and R. Sharma, Strain-tunable ultrastable MoS₂/fluorographene hybrid photodetectors of high responsivity, *ACS Appl. Electron. Mater.* **5**, 5129 (2023).
- [27] See Supplemental Material at <http://link.aps.org/supplemental/10.1103/PhysRevMaterials.8.064004> for more detailed information regarding the schematic diagram of the growth, optical images of the crystals, room-temperature PL fitting of, absorption spectra, evaluation of degree of valley polarization with time, and a table of biexponential fitting of TA kinetics.
- [28] H. Li, Q. Zhang, C. C. R. Yap, B. K. Tay, T. H. T. Edwin, A. Olivier, and D. Baillargeat, From bulk to monolayer MoS₂: Evolution of Raman scattering, *Adv. Funct. Mater.* **22**, 1385 (2012).
- [29] R. Sharma, J. Pandey, K. R. Sahoo, K. S. Rana, R. K. Biroju, W. Theis, A. Soni, and T. N. Narayanan, Spectroscopic correlation of chalcogen defects in atomically thin MoS_{2(1-x)}Se_{2x} alloys, *J. Phys. Mater.* **3**, 045001 (2020).
- [30] J. Zou, Z. Cai, Y. Lai, J. Tan, R. Zhang, S. Feng, G. Wang, J. Lin, B. Liu, and H. M. Cheng, Doping concentration modulation in vanadium-doped monolayer molybdenum disulfide for synaptic transistors, *ACS Nano* **15**, 7340 (2021).
- [31] S. Mignuzzi, A. J. Pollard, N. Bonini, B. Brennan, I. S. Gilmore, M. A. Pimenta, D. Richards, and D. Roy, Effect of disorder on Raman scattering of single-layer MoS₂, *Phys. Rev. B* **91**, 195411 (2015).
- [32] V. K. Rajput, D. Maity, B. K. Deka, T. N. Narayanan, and S. R. G. Naraharisetty, Anisotropic nonradiative recombination of carriers in a few-layered MoS₂ probed by mid-IR ultrafast spectroscopy, *J. Phys. Chem. C* **127**, 13120 (2023).
- [33] B. Upadhyay, R. Sharma, D. Maity, T. N. Narayanan, and S. K. Pal, Ultrafast carrier dynamics in vanadium doped MoS₂ alloys, *Nanoscale* **15**, 16344 (2023).
- [34] K. M. McCreary, A. T. Hanbicki, S. V. Sivaram, and B. T. Jonker, A- and B-Exciton photoluminescence intensity ratio as a measure of sample quality for transition metal dichalcogenide monolayers, *APL Mater.* **6**, 111106 (2018).
- [35] K. M. McCall, C. C. Stoumpos, S. S. Kostina, M. G. Kanatzidis, and B. W. Wessels, Strong electron-phonon coupling and self-trapped excitons in the defect halide perovskites A₃M₂I₉ (A = Cs, Rb; M = Bi, Sb), *Chem. Mater.* **29**, 4129 (2017).
- [36] S. Dal Conte, F. Bottegoni, E. A. A. Pogna, D. De Fazio, S. Ambrogio, I. Bargigia, C. D'Andrea, A. Lombardo, M. Bruna, F. Ciccacci, A. C. Ferrari, G. Cerullo, and M. Finazzi, Ultrafast valley relaxation dynamics in monolayer MoS₂ probed by nonequilibrium optical techniques, *Phys. Rev. B* **92**, 235425 (2015).
- [37] J. Ye, B. Niu, Y. Li, T. Li, and X. Zhang, Exciton valley dynamics in monolayer Mo_{1-x}W_xSe₂ (x = 0, 0.5, 1), *Appl. Phys. Lett.* **111**, 0 (2017).
- [38] Z. Wang, A. M. Sánchez, P. Altmann, D. Sangalli, D. De Fazio, G. Soavi, U. Sassi, F. Bottegoni, F. Ciccacci, M. Finazzi, L. Wirtz, A. C. Ferrari, A. Marini, G. Cerullo, and S. Dal Conte, Intravalley spin-flip relaxation dynamics in single-layer WS₂, *Nano Lett.* **18**, 6882 (2018).
- [39] S. Refaely-Abramson, D. Y. Qiu, S. G. Louie, and J. B. Neaton, Defect-induced modification of low-lying excitons and valley selectivity in monolayer transition metal dichalcogenides, *Phys. Rev. Lett.* **121**, 167402 (2018).
- [40] G. Moody, K. Tran, X. Lu, T. Autry, J. M. Fraser, R. P. Mirin, L. Yang, X. Li, and K. L. Silverman, Microsecond valley lifetime of defect-bound excitons in monolayer WSe₂, *Phys. Rev. Lett.* **121**, 057403 (2018).
- [41] J. Wagner, H. Kuhn, R. Bernhardt, J. Zhu, and P. H. M. Van Loosdrecht, Trap induced long exciton intervalley scattering and population lifetime in monolayer WSe₂, *2D Mater.* **8**, 035018 (2021).
- [42] C. Jiang, W. Xu, A. Rasmita, Z. Huang, K. Li, Q. Xiong, and W. B. Gao, Microsecond dark-exciton valley polarization memory in two-dimensional heterostructures, *Nat. Commun.* **9**, 753 (2018).